Divide-and-conquer strategy with engineered ossification center organoids for rapid bone healing through developmental cell recruitment

Xianzhu Zhang[1,2], Wei Jiang[1,2], Xinyu Wu[1,2], Chang Xie[1,2], Yi Zhang[1,2], Liying Li[1,2], Yuqing Gu[1,2], Zihao Hu[1], Xinrang Zhai[2], Renjie Liang[2], Tao Zhang[2], Wei Sun[1], Jinchun Ye[2], Wei Wei[2], Xiaozhao Wang[1], Yi Hong[2], Shufang Zhang[2], Youzhi Cai[1], Xiaohui Zou[1], Yihe Hu[1], Hongwei Ouyang[1,2] *

Affiliations:

1. Department of Sports Medicine of the First Affiliated Hospital, Zhejiang University School of Medicine, Hangzhou, China
2. Dr. Li Dak Sum & Yip Yio Chin Center for Stem Cells and Regenerative Medicine, Zhejiang University School of Medicine, Hangzhou, China

Abstract

Background: Current approaches for bone repair predominantly target localized delivery of growth factors that are aimed at the coupling of angiogenesis and osteogenesis. However, delayed revascularization and regeneration of critical-sized bone defects are still challenging.

Methods: In this study, we engineer an ossification center-like organoid (OCO) that consist of an inner-core bone morphogenetic and neurotrophic spheroid generated via MSCs-loaded 3D printing, alongside the interstitially distributed outer-shell proangiogenic neurotrophic phase.

Results: The collective implantation of OCOs achieves rapid bone bridging with successive OC-like bone ossicles formation across the bone defect in a “divide-and-conquer” way. Single-cell RNA sequencing analysis unveils a developmentally mimicking stem cell community that dominated with Krt8^{+} skeletal stem cells (SSCs) is uniquely recruited by the pro-regenerative in-situ organoid fusion and maturation. Particularly noteworthy is the specific expansion of Krt8^{+} SSCs concomitant with the simultaneous reduction of Has1+migratory fibroblasts (MFs) post-OCO implantation. Furthermore, cross-species comparisons employing machine learning reveal high resemblance of the relative Krt8^{+}SSCs/Has1^{+} MFs composition in bone regeneration with that in public data from developmental bone tissues.

Conclusion: Our findings advocate an approach akin to “divide-and-conquer” utilizing engineered OC-like organoids for prompt regeneration of large-sized bone defects.

Results

1. CGRP synergistically promoted osteogenesis with BMP-2 at physiological dosage.

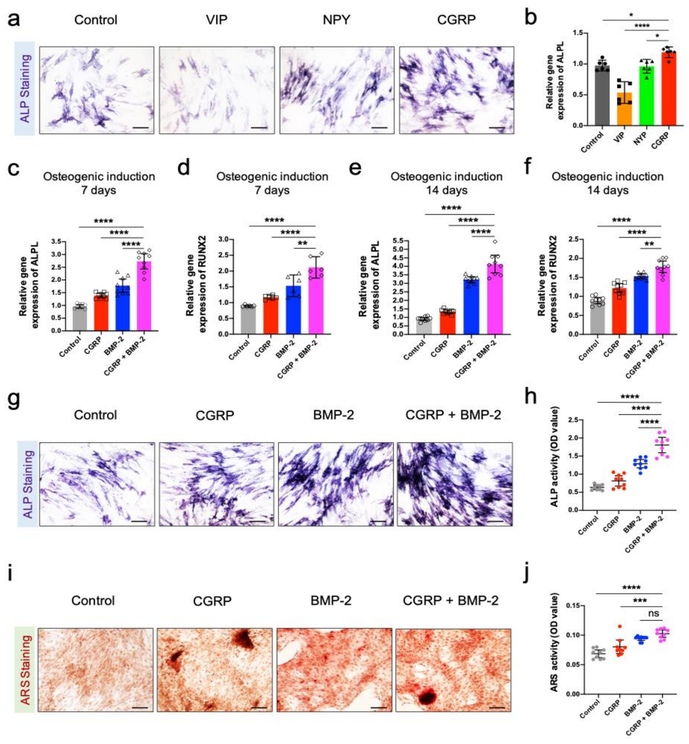


Fig. 1 | CGRP synergistically promoted osteogenic differentiation of MSCs with BMP-2 at physiological dosage. a Alkaline Phosphatase (ALP) staining and **b**. mRNA expression level of ALPL at day 7 after treatment with distinct neuropeptides VIP, NYP, or CGRP, when compared with control osteogenic induction. **c, d** mRNA expression level of ALPL and RUNX2 under osteogenic inductions supplemented with CGRP, BMP-2, or CGRP + BMP-2 for 7 days, respectively. **e, f** mRNA expression level of ALPL and RUNX2 under osteogenic inductions supplemented for 14 days, respectively. **g** Alkaline Phosphatase (ALP) staining and **h** Normalized ALP activity under osteogenic inductions supplemented with CGRP, BMP-2, or CGRP + BMP-2 for 7 days. **i**. Alizarin Red S staining and **j** quantitative OD values under osteogenic inductions for 14 days.

2. All-in-one engineering of ossification center-like organoid with dual-modular neuropeptides.

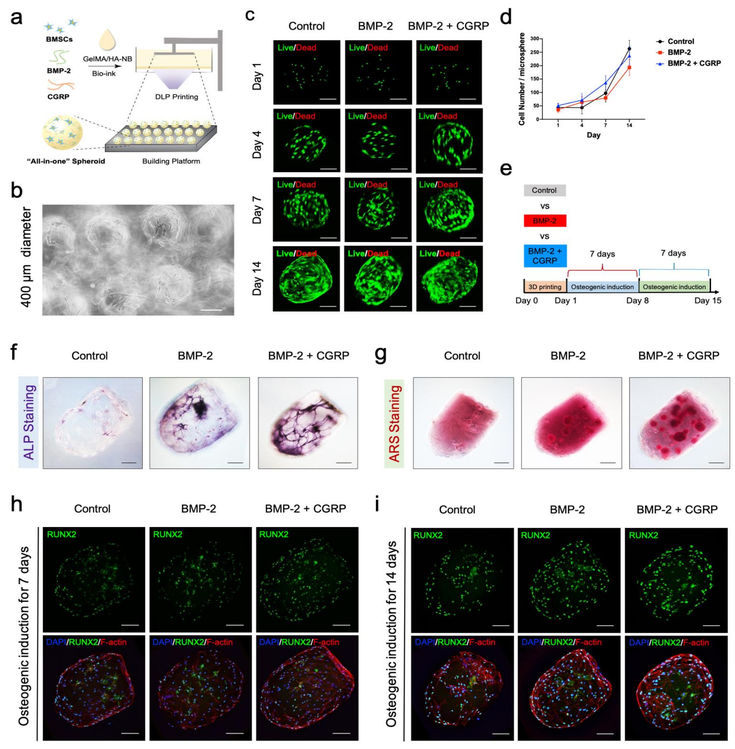


Fig. 2 | 3D printing-based fabrication of “ossification center”-like spheroid with enhanced cell survival and osteogenic potential. a Schematic diagram of MSCs-laden GelMA/HA-NB hydrogel microspheres loaded with CGRP and BMP-2 by DLP 3D printing. **b** MSCs distribution and cell morphology of inside and outside of the microspheres with a diameter of 400 μm after 7 days. **c** Live/Dead staining of MSCs cultured in the vehicle microspheres, or either loaded with BMP-2 alone or combined with CGRP for 1, 4, 7, and 14 days. **d** Quantitative data of cell number within per microsphere among the vehicle microsphere, BMP-2-loaded, and BMP-2 + CGRP-loaded microsphere at day 1, 4, 7, and 14. **e, f** Alkaline Phosphatase (ALP) staining and **g** Alizarin Red Staining (ARS) under osteogenic differentiation of MSCs cultured. **h** and **i** immunostaining of RUNX2 under osteogenic differentiation of MSCs for 7 and 14 days.

3. The divide-and-conquer strategy achieves fast bone bridging with the collective implantation of OC-like bone organoids.

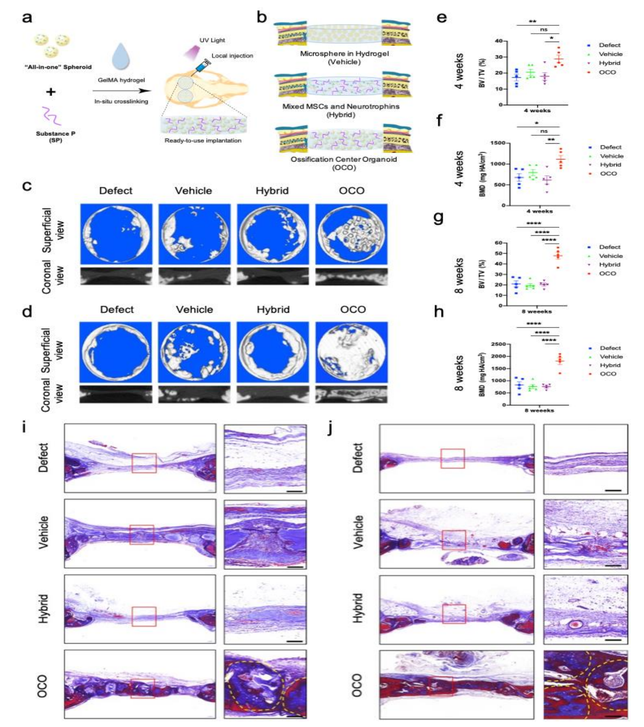


Fig. 3 | OCO implantation achieves fast bone-bridging and full-thickness reconstruction with successive OC-like organoids fusion across the bone defects. a Schematic diagram of the ready-to-use fabrication and in situ crosslinking of OC-like organoids. **b** Schematic illustrating the implantation of the dual-modular hydrogel (Vehicle), Mixed MSCs with Neurotrophins (Hybrid), and Ossification center organoid (OCO) into calvarial bone defect, respectively. **c, d** μ-CT evaluation of bone regeneration at 4 weeks and 8 weeks post-surgery of calvarial defect, respectively. **e** Bone volume fraction (BV/TV) ; and **f** bone mass density (BMD) of regenerated tissues in defect area at 4 weeks post-surgery. **g** BV/TV and **h** BMD of regenerated tissues in the defect area 8 weeks post-surgery. **i, j** Masson’s Trichrome staining of paraffin sections in Defect, Vehicle, Hybrid, and OCO groups at 4 weeks and 8 weeks after calvarial defect, respectively.

4. In situ fusion and maturation of OCOs promote innervation, vascularization, and ossification.

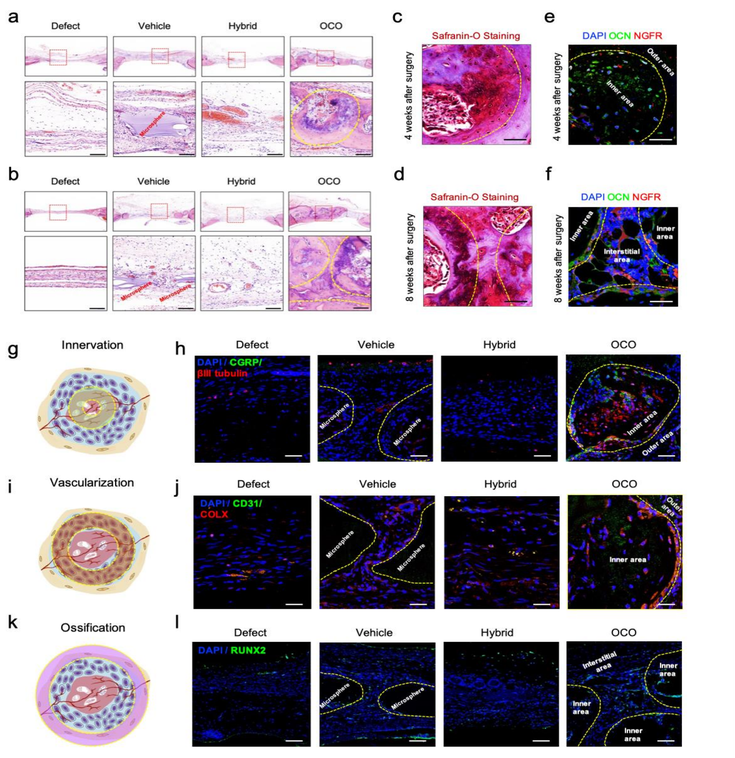


Fig. 4 | In situ fusion and maturation of OCO recapitulates ossification center development with concurrent innervation, vascularization, and ossification. a, b HE staining of paraffin sections in Defect, Vehicle, Hybrid, and OCO groups at 4 weeks and 8 weeks after calvarial defect. **c, d** Safranin-O staining of paraffin sections in Defect, Vehicle, Hybrid, and OCO group at 4 weeks and 8 weeks after calvarial defect. **e** Schematic of neurogenesis in the central area and **f** co-immunofluorescent staining of CGRP and β-III tubulin expression (bar = 20 μm); **g** schematic of angiogenesis in the interlayer and **h** co-immunofluorescent staining of CD31 and COLX expression (bar = 20 μm); **i** schematic of osteogenesis in the outer layer and j co-immunofluorescent staining of OCN and OSX expression (bar = 20 μm); in Defect, Vehicle, Hybrid, and OCO groups at 4 weeks post-surgery.

5. Distinct osteo-lineage cells organize into cell communities that have specific functions.

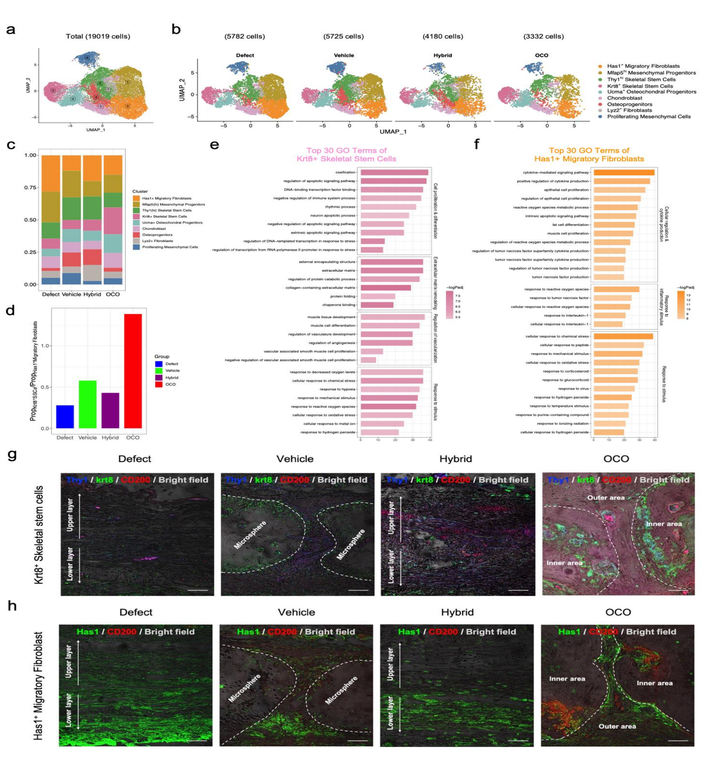


Fig. 5 | Developmental Krt8+ skeletal stem cells are predominantly recruited by the pro-regenerative OC-like organoids during bone regeneration. a UMAP of the 9 OLC subclusters of regenerative bone tissues in Defect, Vehicle, Hybrid, and OCO groups at 2 weeks post-surgery of the calvarial defect. **b** Split UMAP of OLC subclusters. **c** Relative proportion of cells among the above four groups in each subcluster. **d** Relative proportion of Krt8+ SSCs/Has1+ Migratory Fibroblasts among four groups. **e** Top 30 GO terms of Krt8^{+} SSC subset; **f**. Top 30 GO terms of the Has1^{+} Migratory Fibroblasts subset. **g** Co-immunostaining of Krt8 and CD200 expression of paraffin sections of bone regenerative tissue at 4 weeks after defect surgery (bar = 30 μm). **h** Co-immunostaining of Has1 and CD200 expression of paraffin sections of bone regenerative tissue in Defect, Vehicle, Hybrid, and OCO groups at 4 weeks after defect surgery (bar = 30 μm).

6. Developmentally mimicking cell community was orchestrated by proregenerative OC-like organoids.

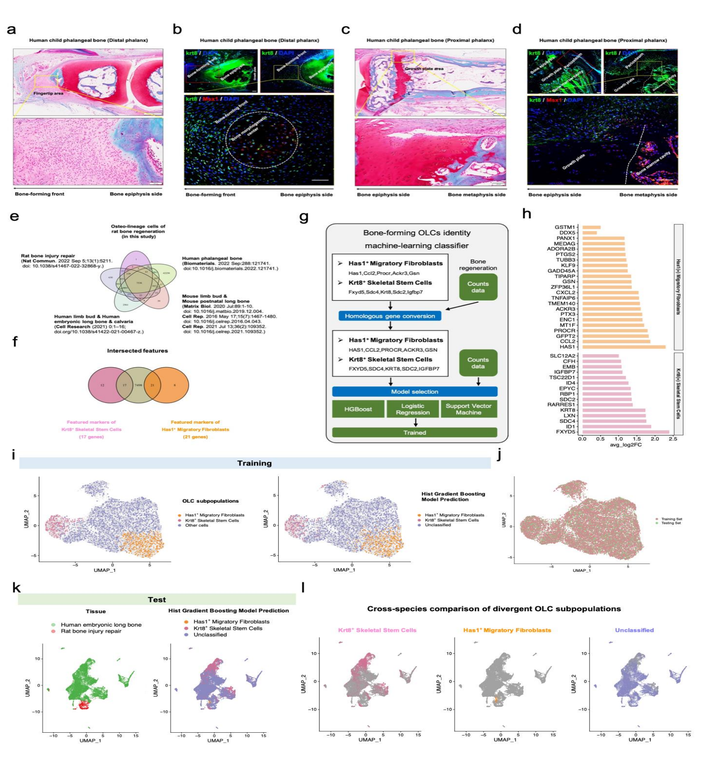


Fig. 6 | Cross-species comparisons by machine learning revealed high resemblance of Krt8+ SSCs in bone regeneration to that in bone development. a and **b** Safranin-O staining and co-immunofluorescent staining of Krt8 and Msx1 in distal phalangeal bone tissues around the epiphysis side; **c** and **d** in proximal phalangeal bone tissues between the epiphysis and metaphysis side. **e** Venn plot showing genes from internal and external datasets. **f** Venn plot showing the process of feature selection. **g** Flow chart illustrating the construction of bone-forming OLCs identity machine learning classifier. **h** Bar plot showing all 38 gene features used in our model. **i** UMAPs of subclustered OLCs used for training and testing. **j** Training and testing set of the internal bone regeneration dataset in our study, with 80% for training set and 20% for testing set. **k** and **l** Integrated and split UMAPs of external datasets showing the prediction results of OLCs by the HGBoost model.

TERMIS EU-Chapter 2026 PALMA DE MALLORCA 21-24 APRIL / SPAIN

termis EUROPE